

## The use of stationarity and nonstationarity in the detection and analysis of neural oscillations

Ville T. Mäkinen,\* Patrick J.C. May, and Hannu Tiitinen

*Apperception and Cortical Dynamics (ACD), Department of Psychology, PO Box 9, FIN-00014, University of Helsinki, Finland  
BioMag Laboratory, Engineering Centre, Helsinki University Central Hospital, PO Box 340, FIN-00029 HUS, Finland*

Received 21 December 2004; revised 25 May 2005; accepted 1 June 2005  
Available online 15 July 2005

Using available signal (i.e., spectral and time-frequency) analysis methods, it can be difficult to detect neural oscillations because of their continuously changing properties (i.e., nonstationarities) and the noise in which they are embedded. Here, we introduce fractally scaled envelope modulation (FSEM) estimation which is sensitive specifically to the changing properties of oscillatory activity. FSEM utilizes the fractal characteristic of wavelet transforms to produce a compact, two-dimensional representation of time series data where signal components at each frequency are made directly comparable according to the spectral distribution of their envelope modulations. This allows the straightforward identification of neural oscillations and other signal components with an envelope structure different from noise. For stable oscillations, we demonstrate how partition-referenced spectral estimation (PRSE) removes the noise slope from spectral estimates, yielding a level estimate where only peaks signifying the presence of oscillatory activity remain. The functionality of these methods is demonstrated with simulations and by analyzing MEG data from human auditory brain areas. FSEM uncovered oscillations in the 9- to 12-Hz and 15- to 18-Hz ranges whereas traditional spectral estimates were able to detect oscillations only in the former range. FSEM further showed that the oscillations exhibited envelope modulations spanning 3–7 s. Thus, FSEM effectively reveals oscillations undetectable with spectral estimates and allows the use of EEG and MEG for studying cognitive processes when the common approach of stimulus time-locked averaging of the measured signal is unfeasible.

© 2005 Elsevier Inc. All rights reserved.

**Keywords:** Electroencephalography; Envelope analysis; Fractals; Magnetoencephalography; Neural oscillations; Ongoing brain activity; Sensory streams; Stationarity; Signal detection; Signal structure; Spectral estimation; Tau rhythm; Wavelets

When a system displays rhythmic activity, one may assume that there are identifiable dynamics in the operation of the system. A large portion of cognitive neuroscience has recently focused on studying oscillations modulated by sensory stimulation and providing a general framework for understanding the oscillatory processes of the brain (e.g., Freeman, 2004a,b; Pfurtscheller and Lopes da Silva, 1999; Varela et al., 2001). The study of the dynamic properties of brain oscillations has gained momentum from methodological advances such as time-frequency transforms, which in principle allow one to observe the approximate frequency and time course of rhythmic brain processes. Unfortunately, the detection of neural oscillations is very difficult with the currently available methods because these oscillations are inherently unstable and separating them from neural and measurement noise is problematic: Already the detection of the presence of rhythmic activity is a major stumbling block for the study of oscillatory brain processes.

The standard method for detecting noise-buried oscillations is spectral estimation: the data are typically divided into short segments whose spectral estimates are averaged to obtain the averaged power spectral density (PSD) where oscillatory processes appear as peaks. There are, however, several reasons why neural oscillations are poorly visible with spectral estimation: (1) Neural oscillations are nonstationary, that is, their frequency and amplitude change over time and phase transients can also occur. Such oscillations are not represented by a single frequency and their power is spread over a range of frequencies: increasing the data segment length (over a certain point) does not yield more accurate information on the frequency of the oscillation, whereas a high number of short time windows allows one to reduce the variance of the average PSD. (2) There are no a priori reasons for assuming that neural oscillations resemble sine waves and the spectral representation of nonsinusoidal waveforms, even when stationary, is spread over several frequencies. (3) Neural oscillations occur within a noise profile that has a roughly one-over-frequency ( $1/f$ ) shape (i.e., low frequencies have more power per frequency unit than high frequencies) and the noise profile can change along the frequency axis. If the signal-to-noise ratio (SNR) is not sufficient, random variations within the noise profile can be

---

\* Corresponding author. BioMag Laboratory, Engineering Centre, Helsinki University Central Hospital (HUCH), PO Box 340, FIN-00029 HUS, Finland. Fax: +358 9 471 75781.

E-mail address: ville.makinen@biomag.hus.fi (V.T. Mäkinen).

Available online on ScienceDirect ([www.sciencedirect.com](http://www.sciencedirect.com)).

greater than the deflection produced by the oscillations, making the detection of the latter very difficult. When SNR is high, the PSD estimate is usually smooth, but one is nonetheless left with an unknown noise profile upon which a broad deflection of an unknown shape representing the oscillation is superposed.

Time-frequency estimation methods such as short-time Fourier transforms, Wigner distributions, adaptive autoregressive moving average (ARMA) models, and discrete and continuous wavelet transforms including matching pursuit algorithms (see e.g., Cohen, 1995; Durka, 2003; Krystal et al., 1999; Mallat, 1998; Pardey et al., 1996) provide, by definition, simultaneous information on the frequency and time evolution of a process. These methods enable the detection of even minute event-related power changes in brain processes. This is achieved by using the prestimulus power level at each frequency band as a reference against which changes are detected and through stimulus time-locked averaging of single-trial time-frequency estimates. However, these two techniques can only be used for studying oscillations modulated by stimulation in a time-locked way; any other oscillations, whether modulated or unmodulated, are beyond their scope. Thus, time-frequency estimates are not especially useful for examining ongoing oscillations; time-frequency estimates at each time point are derived from data of a restricted neighborhood of that time point, whereas spectral estimates are typically derived using much longer data segments and they will consequently have a higher SNR for detecting oscillations. Averaging of time-frequency estimates over time improves SNR in the frequency domain but leads to similar results as traditional spectral estimates without providing major advantages. Further, recent examinations (Mäkinen et al., 2005; Yeung et al., 2004) have shown that the currently employed time-frequency methods are not suitable for distinguishing between modulations of ongoing oscillations and the emergence of evoked responses.

While nonstationarities of neural oscillations pose a major problem in spectral estimation, they are, in fact, their characteristic feature. Here, instead of considering nonstationarity a problem, we introduce fractally scaled envelope modulation (FSEM) estimation which exploits this inherent property in the detection and analysis of neural oscillations. The amplitude envelope of a stationary oscillation is a line with zero slope, whereas nonstationarities of an oscillation are manifested as deflections in the envelope curve. In FSEM, the envelopes for each frequency are obtained via continuous wavelet transforms and the behavior of the envelope curves is captured through appropriate spectral estimation. The method results in a two-dimensional signal representation (frequency vs. envelope modulation frequency) where the examined frequencies are of equal scale but, importantly, neural oscillations can be identified by their modulation structure differing from that of the noise at neighboring frequencies. Although quite different in implementation, FSEM is functionally closer to spectral estimation than to time-frequency methods in providing a compact representation of large amounts of data and in revealing noise-buried oscillations. However, unlike spectral estimation, FSEM is able to describe the temporal structure of oscillations. Complementing FSEM, designed to reveal nonstationary oscillations, we also develop spectral estimation methodology for brain research purposes by introducing partition-referenced spectral estimation, PRSE (for a preliminary exposition, see Mäkinen et al., 2004b), a technique which removes the  $1/f$  slope of the noise and leaves near-stationary oscillations as distinct peaks in the estimate. In the following, we begin by describing spectral estimation and its extension PRSE, and then proceed to FSEM. The methods are used

to examine ongoing brain activity obtained with MEG from human auditory brain areas during auditory stimulation. With the focus of our investigation being on ongoing activity, none of the data analysis in this study is performed in a stimulus time-locked manner. We demonstrate that despite this, FSEM can also describe auditory-evoked activity in virtue of this being a form of modulation of the MEG signal.

## Methods

### *Measurements, subjects, data collection, and basic analysis*

Ten healthy human subjects were studied with their informed and written consent. The study was approved by the Ethical Committee of Helsinki University Central Hospital. The measurements were carried out in a magnetically shielded room with a 306-sensor MEG device (Elekta Neuromag Oy, Finland). The subjects watched a silent film and were under instruction to ignore the auditory stimuli. The stimuli were binaurally delivered 750-Hz tones of 50-ms duration (with 5-ms linear onset and offset ramps) adjusted to 80 dB (sound pressure level, A-weighted) and presented >800 times using an onset-to-onset inter-stimulus interval of 1200 ms (corresponding to ~16 min of raw data). Two empty-room measurements with the same settings were also performed. The data were collected using a sampling rate of 600 Hz and a pass-band of 0.03–200 Hz. Online averaging was performed with epochs rejected if the electrooculogram exceeded 11501  $\mu$ V or if the amplitude of the MEG within a trial exceeded 130001 fT/cm. For each subject, data were analyzed from the (planar) gradiometer pair which displayed the largest-amplitude N100m response. All the analyses described below were carried out for data from each sensor of the pair separately, after which vector sums  $x = \sqrt{(x_1)^2 + (x_2)^2}$  of the analysis results were calculated. This was done because each sensor measures only one orthogonal component of the spatial gradient of the magnetic field (Knuutila et al., 1993). Data were visually inspected and, in two subjects, a particularly noisy data segment from a single sensor was excluded from further analysis. To simplify subsequent analyses, the data were upsampled to 1000 Hz. Spectral estimation was performed using zero-padded 4096-point FFT periodograms with time windows of 500, 1000, and 2000 ms. With a high number of spectral estimates providing a smooth average PSD, we focused on the frequency resolution and used a boxcar window for spectral estimation. The results of the spectral estimation are of the form  $10 \times \log_{10}(\text{Power}) [(fT/cm)^2 / \text{Hz}]$  but for convenience are referred to simply as Power (dB). For artefact rejection, time windows whose standard deviations (SD) exceeded double the mean SD over all time windows were rejected from spectral estimation. The data windows were detrended (with linear least squares fit) prior to calculation of the spectral estimates. This preprocessing was used in all following spectral estimates (e.g., within FSEM). The time windows of the PSD estimation were spaced at half the distance of their length. The time windows were therefore overlapping, and while this is partially redundant it also reduces the data loss due to artefact rejection caused by local disturbances.

### *Partition-referenced spectral estimation: basic description*

Partition-referenced spectral estimation, PRSE, is a new technique we propose for removing the  $1/f$  noise slope inherent in spectral estimates of brain activity. It is based on the observation

that as the length of the time window increases from which a spectral estimate is calculated, the spectral peaks of approximately stationary oscillations become sharper and higher in amplitude. This effect is considered here in more detail using the periodogram, the basic spectral estimation method which is a magnitude-squared discrete Fourier transform of a signal with power scaled according to signal length. The periodogram can be considered to operate by filtering the signal with sine and cosine functions that match each estimated frequency. These filters correspond to a bank of band-pass filters, with the output of each filter producing a frequency point (bin) in the spectral estimate (see, e.g., Hayes, 1996). The bandwidth of each filter is inversely proportional to the length of the signal. When the periodogram is calculated using a short time window the filters have large bandwidths and several filters of the periodogram have considerable overlap with any single-frequency oscillation. Thus, in the obtained spectral estimate, the power of the oscillation is spread over a wide frequency range. When a longer time window is used, the filter bandwidths are narrower and hence the frequency of the oscillation overlaps effectively with fewer filters. The power is now concentrated around fewer frequency points with higher amplitude.

The prerequisite for this effect is that the oscillation is approximately stationary within the time windows from which the estimate is calculated. If the signal is noise (i.e., each value of the signal is independent from previous values), the PSD values reflect stochastic coincidence between signal values and the filters of the periodogram and are generally independent of the used window length. Therefore, if we have data where an oscillation occurs within noise and we divide a PSD estimate of the data with a PSD obtained using a shorter time window, the slope of the noise is removed. As the peak of the oscillation is of higher amplitude in the PSD obtained with the longer time window, a deflection signifying the presence of rhythmic activity remains even after the division.

In PRSE, we use the PSD of a time window as the nominator and the average of the PSD estimates calculated from the partitions of the same time window as the denominator (=reference PSD), which ensures that the PSD estimate and its reference contain the same data. The most important factor determining the outcome of PRSE is the level of stationarity of the oscillations within the examined signal. That is, when window length is increased and the peak of an oscillation is no longer observed in PRSE, it indicates that the oscillation is spread over a wider frequency band than the filter bandwidth of the partitioned window. Therefore, by using a range of window lengths, PRSE allows one to obtain a measure of the duration of the stationarity of an oscillation.

#### *PRSE: implementation and technical considerations*

In the current study, PRSEs were calculated using 25 logarithmically spaced time window lengths in the 500- to 4000-ms range. Time windows were rejected if their SD exceeded double the mean SD calculated over 2000-ms time windows for each subject. The same half-overlapping window spacing as in the direct PSD

estimation was used. For each time window, the reference spectrum was obtained by halving the time window into two parts prior to calculating the periodogram. FFT length was selected to be the closest power of two greater than twice the number of samples of the nonpartitioned time window. PRSEs calculated using shorter time windows were upsampled to the length of the PRSE of the longest time window. This is computationally much more efficient than using the same FFT length for all time windows.

The lowest oscillation frequency (besides DC) whose power can be estimated with spectral estimation has a cycle length (inverse of frequency) equal to the length of the analyzed time window. Hence, as the reference PSD is not valid for frequencies with cycle lengths above the length of the partitions, the corresponding frequency points were discarded from the estimates. Oscillations have a characteristic shape in PRSE where the peak of the oscillation is surrounded by power reductions. This follows from the full-window PSD estimate containing the same power as the partition reference, but with the power being more concentrated in the former. This characteristic shape of PRSE has the effect that peaks not accurately aligned, for example over subjects, effectively cancel each other out in grand-averaging. To form averages of PRSEs of heterogenic data, one needs to use a nonlinear transform which enhances the positive peaks more than the surrounding power reductions. As the mean value of the PRSE is unity, a straightforward transformation is to calculate moments (i.e., powers) of the data: these have a nonlinear effect in increasing the >1 values more than reducing the <1 values, which prevents the cancellation effect in averaging. In the present study, the 10th moment was used in the grand average. The value of the moment is arbitrarily selectable, with the higher values emphasizing the peaks more but also making the estimate more susceptible to noise.

The grand average PRSE for single-sensor data  $x$  can be written as shown in Eq. (1), where  $P$  is the number of accepted data windows with onset times  $t_p$ , and PSD is the periodogram algorithm including preprocessing of data. The window length  $L$  is an even number (25 instances were used here; see above), the moment is  $m$ , and  $N$  is the number of subjects. For gaining single-subject probability values for PRSE and FSEM, we used an a priori assumption that the data are normally distributed. The variance of this distribution was estimated from the selected baseline (further validated by the results in Fig. 3 where the data contain no structure if the signal consists of noise only). The probabilities were then obtained from the two-tailed complement of the normal cumulative distribution function. A peak whose amplitude was at least 3.3 SDs above the mean of the signal (corresponding to  $P < 0.001$ ) was considered significant. For calculating the SD, the 20- to 40-Hz range was used because it contained no peaks. Finally, we might note that the spectral slope can also be removed from the spectrum of the full-length time window with subtraction of the reference spectrum rather than with division as used here. After subtraction, however, the magnitude of the noise in the estimate remains  $1/f$ -dependent on frequency, which does not facilitate the meaningful use of nonlinear techniques in grand-averaging.

$$\text{PRSE}_{\text{grand average}} = \frac{1}{N} \sum_{n=1}^N \left( \frac{\sum_{p=1}^P \text{PSD}[x(t_p), x(t_p + L - 1)]}{\frac{1}{2} \left( \sum_{p=1}^P \text{PSD}[x(t_p), x(t_p + L/2 - 1)] + \sum_{p=1}^P \text{PSD}[x(t_p + L/2), x(t_p + L - 1)] \right)} \right)^m \quad (1)$$

### Fractally scaled envelope modulation estimation: basic description

Fractals are objects that display self-similarity over different scales, examples of these being found widely in nature and mathematics (e.g., Barnsley, 1988). Wavelets exhibit fractal behavior because, regardless of the scale (i.e., center frequency or cycle length of a wavelet), the shape of the wavelet remains the same. In contrast, the filter shape in Fourier analysis changes with increasing frequency so that it contains more cycles of the corresponding frequency. With wavelets the filter shape is constant, but because of the definition of frequency, the

bandwidth of the filter increases with decreasing scale (increasing frequency). This is the fundamental difference between Fourier (e.g., periodogram) and wavelet analysis and serves as the starting point of fractally scaled envelope modulation (FSEM) estimation.

The first step in FSEM (Fig. 1) is a continuous wavelet transform (CWT, e.g., Addison, 2002; Mallat, 1998; Torrence and Compo, 1998) of the data: If the wavelet is complex, the modulus of the wavelet coefficients describes the time course of the amplitude envelope of that frequency. If the wavelet has a real part only, the amplitude envelope is obtained through Hilbert-

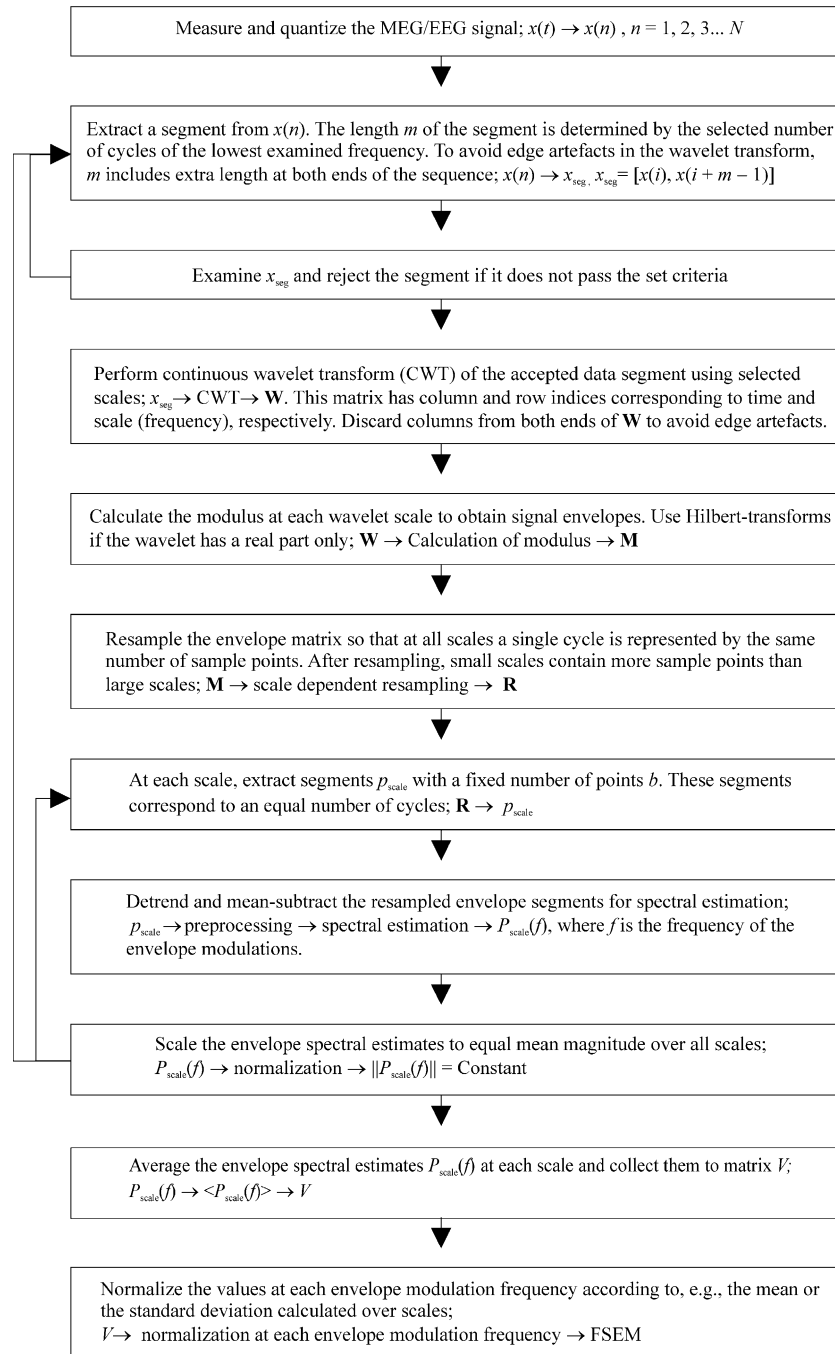


Fig. 1. Flow chart of the calculation stages of FSEM. The returning arrows refer to loops in the algorithm.

transforming the wavelet coefficients and taking the modulus of the transform. As the CWT is fractally scaled, the envelope fluctuations of the wavelet transform and the cycle length of the corresponding scale have the same ratio at all scales. That is, the analysis can be performed to the same resolution at every scale when the envelopes of the wavelet transform are resampled so that at all scales the same number of samples corresponds to one cycle. After this operation, the number of samples at each scale is thus no longer equal; larger scales (lower frequencies) contain less data than smaller ones, which is in line with the amount of information the signal at each scale can have. This can readily be observed from the densities of the wavelet coefficients per scale in a discrete wavelet transform (Addison, 2002; Mallat, 1998).

The fluctuation of the amplitude envelopes obtained through the CWT is efficiently examined with spectral estimation. To retain fractal scaling, the PSD estimates of the envelopes need to be calculated using equal-length data windows at each scale. These PSD estimates are then averaged for each scale. The number of data windows that are available for the calculation of the PSD estimates is higher with smaller scales. This does not affect the shape of the PSD but, after averaging the PSDs at each scale, the smaller-scale PSDs have a lower noise level. The mean power of the PSD estimates obtained at larger scales (lower frequencies) tends to be greater than that obtained at smaller scales, as it approximately follows the  $1/f$  power distribution of a PSD calculated directly from the data. However, the actual power is not of interest but, rather, how this power is distributed in the PSD estimates of the envelope fluctuations. Therefore, when we normalize the envelope PSDs at each scale to be of equal mean power, the outcome is a two-dimensional (frequency vs. envelope modulation frequency) representation of time series data describing specifically, for each analyzed frequency (wavelet scale), the distribution of envelope modulations in respect to its cycle length. In the following, this distribution is simply referred to as the structure of the signal at that frequency, where the frequency is the center pass-band frequency of the used wavelet.

The PSD of a neural signal typically exhibits decreasing power with increasing frequency as does the PSD of the envelope modulation, which is likely to represent so-called multifractal behavior (Mandelbrot, 1999). Thus, the current PSD estimates have decaying power with increasing envelope modulation (EM) frequency (modulations per cycle) and the detection of a peak from the possibly noisy PSD slope can be difficult. However, unlike with the PSD obtained directly from the data, we now have a PSD for each frequency. These PSDs differ from each other only according to the distribution of the spectral power of the envelope modulations. Thus, the values reflecting modulation structure differing from that of the noise can be readily identified with respect to other values of the corresponding EM frequency. The simplest way of doing this is to subtract the EM frequency values averaged over the scales from all the values of the corresponding EM frequency. Here we used SD-based referencing, as it has the advantage of directly providing a probability value for each sample (see previous section). The calculation stages described in this section comprise FSEM estimation and are presented schematically in Fig. 1. In Fig. 2, we use simulated data to demonstrate the ability of FSEM to describe the structure of oscillations. The structure described by EM frequency can be quantified as follows: Duration of modulation in seconds [s] = (inverse of modulations-per-cycle [unitless])  $\times$  (inverse of frequency [Hz = 1/s]).

### FSEM: implementation and technical considerations

In CWT, the distribution of the wavelet scales (frequencies) is arbitrarily selectable within the limits of the data record length and sampling rate. The CWT multiplies the size of the original data with the number of the scales and may thus pose computational limits. Here the wavelet scales were set 1 Hz apart. From a signal decomposition view this is redundant, but the denser the scaling, the more suitable it is for signal detection purposes. Three wavelets were employed: a second derivative of Gaussian wavelet (DOG-2) for high temporal resolution; a complex Morlet wavelet (Morlet-6) with a wave number of six ( $f_0 = 0.95$ ) as a compromise between time and frequency resolution; and a complex Morlet (Morlet-12) wavelet with a wave number of 12 ( $f_0 = 1.9$ ) for high frequency resolution. The calculation of the CWT was performed with the commonly employed, computationally efficient method of calculating Fourier transforms of the data (via FFT), multiplying these by the discretized Fourier transforms of the scaled wavelets (for which symbolic transforms are known), and then performing an inverse Fourier transform on the product. The computational cost of FSEM is, nonetheless, likely to be mainly determined by the calculation of the CWT (in the current implementation, 80% of the total calculation time). The CWT was calculated using windows of 50, 100, and 200 cycle lengths of the largest scale used with additional ten cycles at both ends of the data segments. The data of the ten cycle lengths at both ends were discarded after CWT to avoid edge artefacts. The resulting data loss was limited to the ends of the full-length data record with the data segmentation performed with overlapping segments according to length of the discarded data portion. If the SD of the window exceeded double the mean SDs of all the data windows, it was excluded from analysis. In order to limit the window length, the examined frequencies were set to begin from 5 Hz. The highest examined frequency was 100 Hz. All the scales of the CWT data were resampled so that a single cycle of an oscillation was represented by 10 samples and, as the wavelets are band-pass filters, no separate low-pass filtering was required to avoid aliasing in the resampling. The windows used in the calculation of the envelope modulations were thus 500, 1000, and 2000 samples corresponding to 50, 100, and 200 cycles, respectively. The periodograms were calculated using 4096-point FFTs and the estimates of each scale were subsequently averaged separately for each subject. The resulting matrixes were normalized at each EM frequency by subtracting the mean calculated over scales and then dividing with the SD calculated from the desired frequency (scale) range.

A central question for the ability of FSEM to identify oscillatory processes is how the structure of the noise depends on frequency. For example, is the structure of noise the same at 10 Hz and 100 Hz? We used simulated data to examine whether the envelope power distribution exhibits frequency dependence with FSEM. We generated sequences (of the same length as the current single-sensor MEG data) with different noise profiles: white noise,  $1/f$  (pink) noise, and two-component noise whose PSD slope closely resembles that of the MEG data (Fig. 3a). A close fit to the PSD distribution of MEG noise was obtained by using noise with a  $1/f^{1.2}$  slope up to 50 Hz and white noise from thereon.

The initial visual inspection of the FSEMs calculated from the simulated signals suggested no dependence of the noise structure on frequency. Quantitative analysis was performed by evaluating, for all EM frequencies, the slope of a linear (least squares) fit

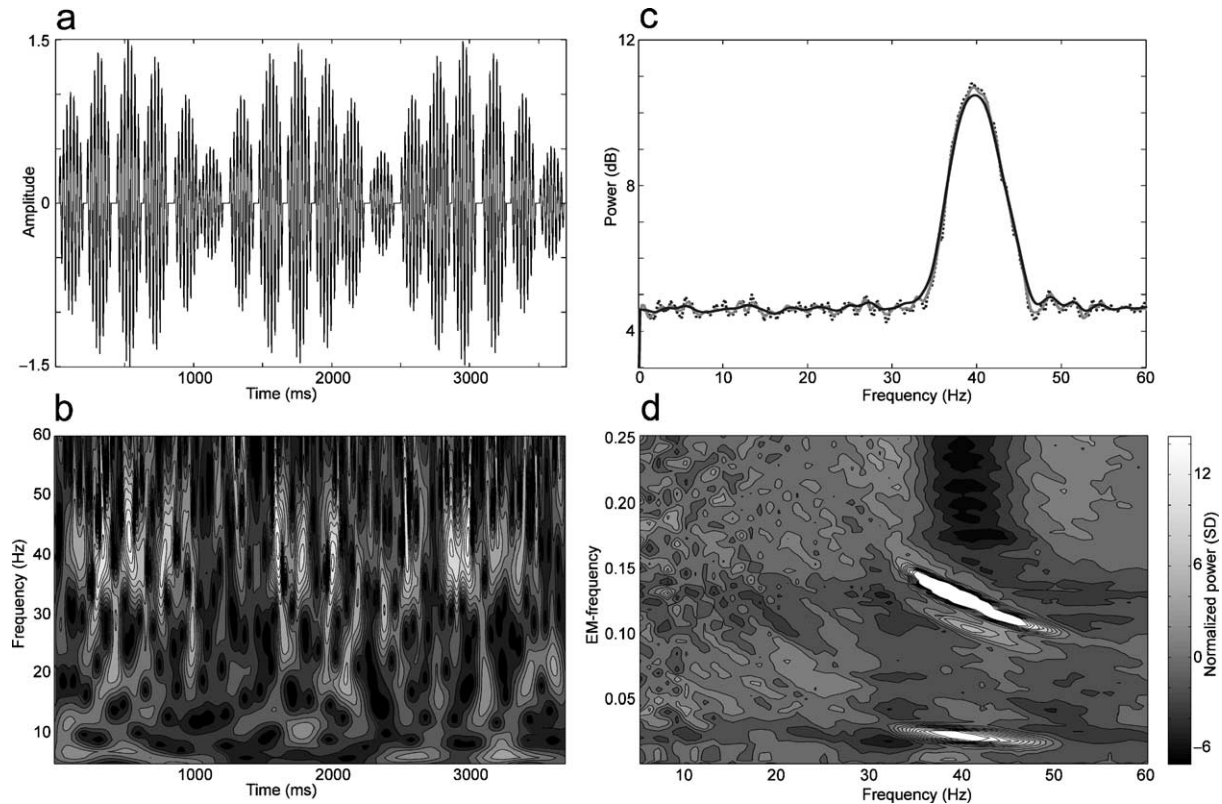


Fig. 2. Analyses of simulated data. (a) A sample of the simulated signal: a 40-Hz oscillation modulated at distances of 8 and 48 cycles corresponding to envelope modulation (EM) frequencies of 0.125 and 0.021 modulations per cycle, respectively (each modulation is separated by a varying-length, zero-level signal). The signal is embedded in white noise with standard deviation (SD) of twice the mean peak amplitude of the 40-Hz oscillation. The simulated signal is of the same length as the single-sensor MEG data of the current study. (b) A sample of the continuous wavelet transform (CWT) of the signal obtained with a Morlet-6 wavelet is shown. The scaling is arbitrary, and here the wavelets were set to have equal energy at all scales (brighter values signify higher magnitude). Although traces of the 40-Hz oscillation can be observed, the signal-to-noise ratio is not sufficient for determining the signal structure directly from the CWT. (c) Spectral estimates with a periodogram using 500-, 1000-, and 2000-ms time windows (solid black, solid gray, and dashed black curves, respectively) contain a prominent peak at 40 Hz. Because the signal does not comprise a stable 40-Hz oscillation, it is not described by a single frequency and therefore the spectral peak is broad regardless of the width of the analysis time window. (d) The FSEM plane (Morlet-6 wavelet and 100 cycle length window) clearly shows a process at 40 Hz whose structure differs from that of noise. Further, unlike in panels b and c, the EM frequencies of the modulations of the oscillation are revealed.

over scales (frequencies). Were these slopes systematically to differ from zero, this would reveal that the structure of noise depends on frequency according to some (monotonic) function. The slopes of the fits, plotted in Fig. 3b, are equally distributed around zero, indicating that there is no dependence of the structure of noise on frequency. One might emphasize that the small magnitudes of the slopes (all values are below  $10^{-14}$ ) demonstrate that the current implementation of FSEM provides consistent estimates. In the case that noise structure in FSEM would in some manner depend on frequency, the detection of oscillatory processes could be facilitated by either detrending or high-pass filtering over scales at each EM frequency to remove the dependence.

## Results

### Spectral estimates and basic data characterization

The spectral estimates of MEG data obtained using 0.5-, 1- and 2-s time windows grand-averaged over the subjects as well as the spectral estimate of the empty-room measurements are shown in

Fig. 4. The 50-Hz mains noise illustrates how increasing the window length sharpens and increases the spectral peak of an approximately stationary oscillation. Aside from containing the 50-Hz peak, the empty-room and grand-averaged spectral estimates display different slope characteristics and thus the empty-room spectrum is not likely to be particularly useful as a reference for data obtained from subjects. The grand-averaged PSDs display the  $1/f$  shape, and a broad peak centered at around 10 Hz is easily observable. This peak corroborates previous results showing that human auditory areas exhibit a tau rhythm visible in MEG (Lehtelä et al., 1997; Bastiaansen et al., 2001). However, if the spectra are not as smooth as in the current grand average, it may be difficult to identify peaks from the PSD signifying rhythmic activity and further their statistical testing is complicated because the absolute value at a PSD peak is likely to depend more on the underlying noise slope than on the amplitude of the oscillatory process in question.

PRSE alleviates these problems in identifying and quantifying PSD peaks in noise. The grand-averaged PRSEs for the 25 window lengths spanning 0.5–4 s are shown in Fig. 5a. The 50-Hz noise is seen as a very strong component whose PRSE magnitude is little affected by window length. The 10-Hz activity

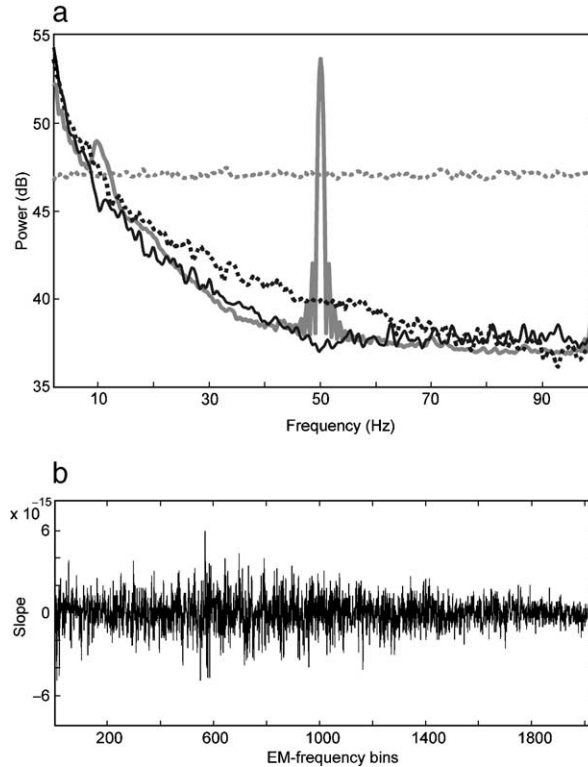


Fig. 3. FSEM behavior for simulated signals with three noise profiles. (a) The power spectra of the test signals are shown: a white noise signal (dashed gray curve), a signal with  $1/f$  power distribution (dashed black curve), and a two-component signal consisting of  $1/f^{1.2}$  and white noise for frequencies below and above 50 Hz, respectively (solid black line), which most closely resembles actual MEG data (solid gray curve). The power spectra were obtained with a periodogram using a 1000-ms time window. FSEM estimates were calculated using the simulated signals in order to examine whether FSEM artefactually displays structure for noise depending on scale. At each EM frequency the values were normalized to a mean value of 1 and linear fits over scales were calculated. For all signals, the slope magnitudes were below  $10^{-14}$  and equally distributed around zero, demonstrated in panel b for the two-component signal (there are 2049 EM frequency bins, as the used FFT length was 4096). Thus, FSEM estimates for noise are independent of scale, and therefore any structure found in the FSEM plane must be due to processes other than noise.

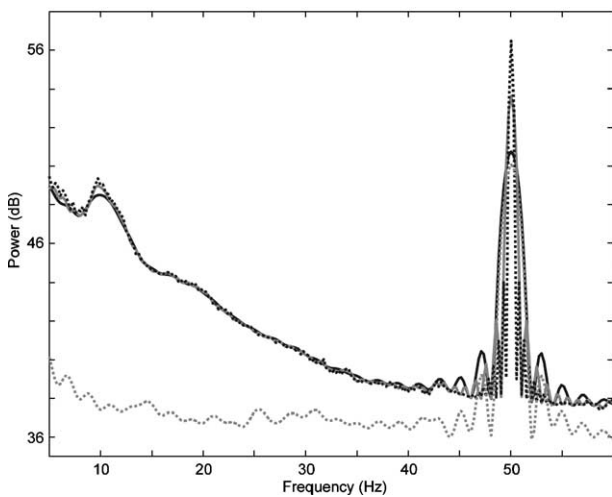


Fig. 4. Grand-averaged spectral estimates of MEG data from the auditory brain areas. Estimates were obtained with 500-, 1000-, and 2000-ms time windows (solid black, solid gray, and dashed black curves, respectively) and an empty-room power spectrum was obtained with a 500-ms time window (dashed gray curve). The grand-averaged spectra display decreasing power with increasing frequency, a broad peak at 10 Hz, and a prominent peak of the 50-Hz mains noise.

is clearly seen with short windows but is poorly visible when the window length is over 1 s. The amplitude of the 10-Hz neural oscillation and the 50-Hz noise as a function of window length are shown in Figs. 5b and c, respectively. The differences in the shape and magnitude of the curves reflect the differences in the stationarity of the processes as well as in the accuracy of the alignment of the processes over subjects. With long time windows and low frequencies the PRSE values are noisy, which is caused by the lower number of estimates and the large magnitude variation of the approximately  $1/f$ -shaped spectrum at low frequencies. Further, in the periodogram estimation, shorter time windows correspond to broader filter bands and therefore provide smoother estimates.

As illustrated in Figs. 5a and b, the 10-Hz neural oscillation is best observed with the shortest time windows. Hence, the average from the five shortest window lengths (Fig. 5d) was used to evaluate the data from individual subjects. Two examples of single-subject PRSEs are shown in Fig. 5e, demonstrating the large inter-individual differences: Six of the ten subjects had a distinct peak in the 9- to 12-Hz range, one displayed a significant peak at 17 Hz, and three showed no indication of rhythmic activity. The double peak at around 10 Hz in the grand average PRSE (Figs. 5a and d) is due to four subjects having a peak at 9–10 Hz while in two subjects the peak was at 11–12 Hz. When compared to spectral estimation with its difficulty in revealing oscillation peaks from the  $1/f$ -shaped noise slope, these results

highlight the ease with which PRSE reveals neural oscillations and their inter-subject heterogeneity.

Besides ongoing oscillations, we observed prominent auditory-evoked responses (Fig. 6). As these responses are transient and of short duration (resembling the impulse response), their power is spread over a wide frequency range, and thus they are not effectively characterized via spectral estimates. A detailed description of the auditory event-related processes in the time-frequency

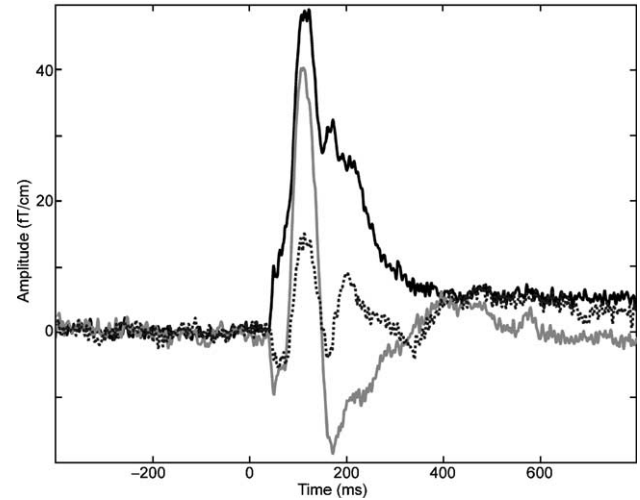
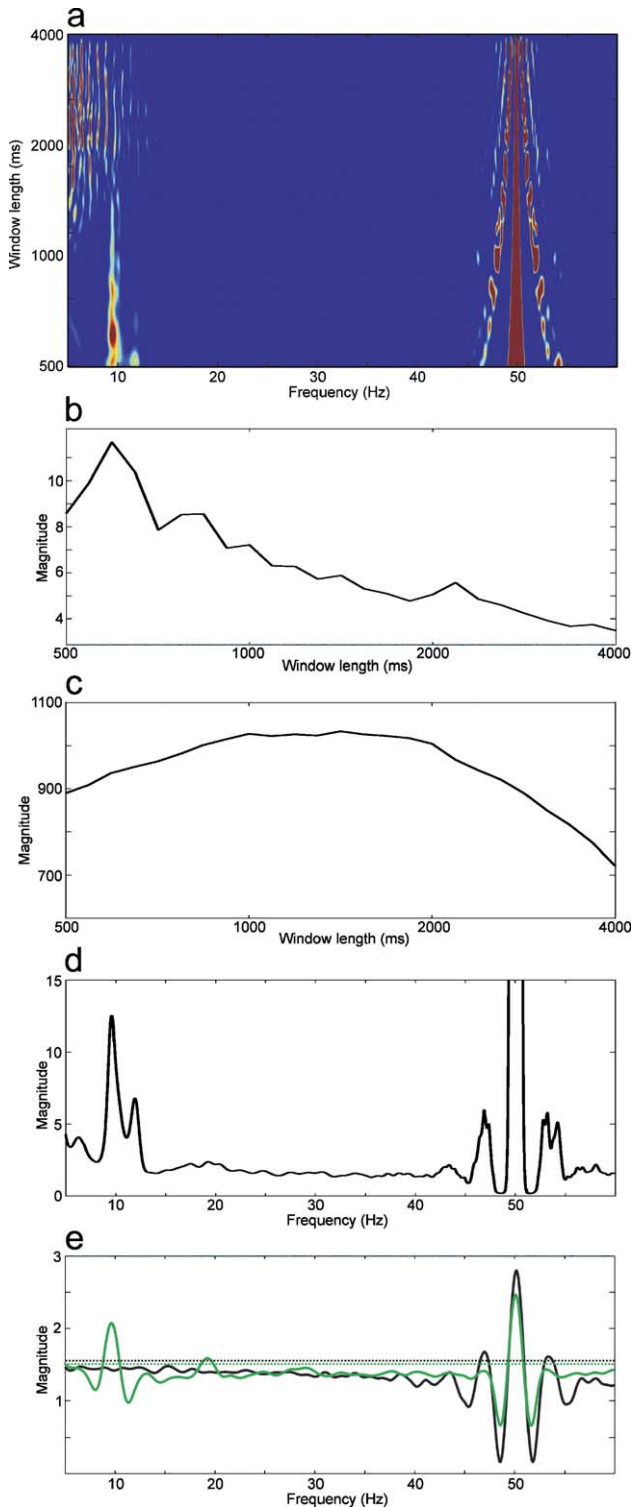


Fig. 6. Grand-averaged auditory-evoked MEG responses. The data are from the gradiometer sensor exhibiting the largest auditory response (gray curve) and its orthogonal sensor pair (dashed black curve). Also shown is the vector sum from this pair (solid black curve). The responses are prestimulus baseline corrected and unfiltered.

plane is provided elsewhere (Mäkinen et al., 2004a). However, unlike analyses performed with the methods introduced here, these examinations leave uncharted the brain activity that is not modulated in a stimulus time-locked fashion.

#### FSEM estimation of the data

Grand-averaged FSEM planes are presented in Figs. 7a–c. These planes have three processes with structure differing from noise: the 50-Hz mains component, auditory-evoked responses, and neural oscillations. The first two have a specific, known spectrotemporal structure and they illustrate the general properties of the FSEM planes: In the plane obtained with the Morlet-12 wavelet of high frequency resolution (Fig. 7a), the power of the 50-Hz mains noise is concentrated in a narrow frequency range and at low envelope modulation (EM) frequencies. As shown in Fig. 7a, if oscillatory processes have power concentrated at low EM frequencies, power at high EM frequencies will be reduced. This follows from the used normalization which ensures that all frequencies have equal mean power over EM frequencies. The effect of the 50-Hz component also leaks into neighboring

Fig. 5. Partition-referenced spectral estimation (PRSE) of the auditory MEG data. (a) The plane shows the grand-averaged PRSEs for different window lengths calculated with 10th moments. The 50-Hz mains noise is prominent at all window lengths. The 10-Hz oscillation is visible only with window lengths up to 1.5 s, which provides an estimate of the duration of its stationarity. The scale of panel a is displayed in panels b–d. (b and c) The 10-Hz and the 50-Hz PRSE magnitudes, respectively, are mapped as a function of window length. (d) The average PRSE magnitude over the first five window lengths is shown. The spectral peaks are much more pronounced than in the spectral estimates (see Fig. 4). (e) Large inter-individual differences are demonstrated by the PRSEs from two subjects. One subject (black curve) displays no peaks and the other (green curve) has peaks at 9.6 Hz and 19.2 Hz (the latter is likely to be a harmonic of the former). The horizontal dashed lines indicate the individual limits of significance for the peaks.

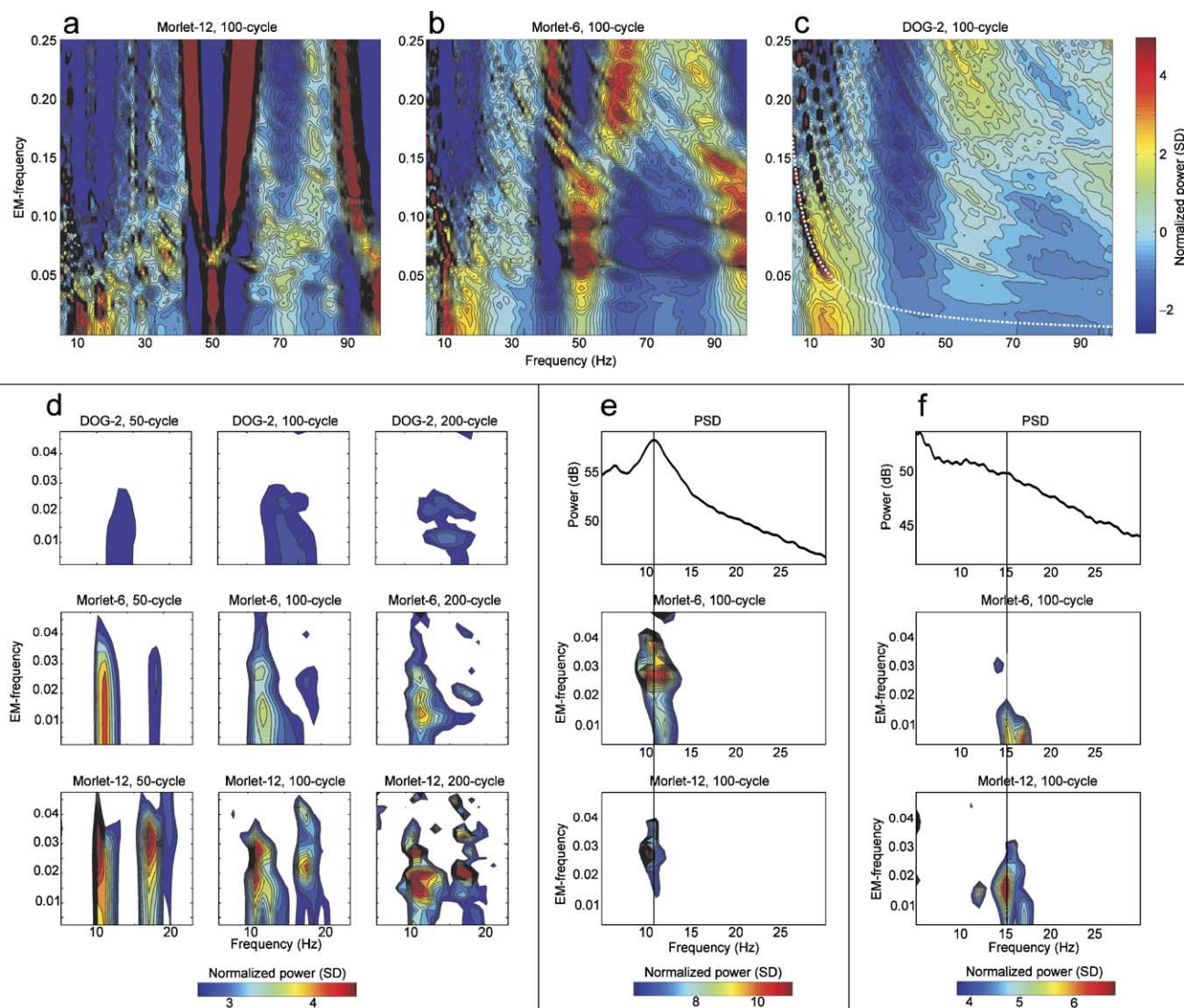


Fig. 7. FSEM planes of the MEG data from the auditory brain areas. (a–c) Grand-averaged FSEM planes obtained using 100 cycles at each scale are shown. The planes are in the order of decreasing frequency resolution and increasing time resolution (from left to right: Morlet-12, Morlet-6, and DOG-2 wavelets used in the initial time-frequency transformation). A high frequency resolution reveals oscillatory processes of a high level of stationarity (e.g., 50-Hz mains component), whereas a high temporal resolution emphasizes processes localized in time (e.g., auditory-evoked responses). (c) The constant inter-stimulus interval of auditory stimulation is represented by the dashed white curve in the FSEM plane. Neural oscillations are visible in all FSEM planes as concentrations of power at low EM frequencies in the 10- to 20-Hz range. (d) The visibility of oscillatory processes with different wavelets and window lengths is demonstrated (rows: wavelets DOG-2, Morlet-6, and Morlet-12; columns: 50, 100, and 200 cycle windows). The frequency resolution of the FSEMs increases from top to bottom and EM frequency resolution increases from left to right. In each panel, the region from the grand-averaged FSEM plane including oscillatory processes is shown (only values of  $P < 0.005$  are displayed). Oscillatory processes can be observed at approximately 10 Hz and 17 Hz with the level of detail depending on the FSEM parameters. (e and f) Data from two subjects examined with spectral estimation and FSEM are shown. The top, middle, and bottom panels display the PSD, the Morlet-6 FSEM, and the Morlet-12 FSEM, respectively. When, as in panel e, the PSD displays a discernible peak (at 11 Hz), the FSEM plane also shows oscillatory activity in the same frequency range. In contrast, when the PSD contains no identifiable spectral peaks, as in panel f, FSEM is able to pick up rhythmic activity (at 15 Hz;  $P < 0.001$ ). (e) The Morlet-6 displays the oscillatory process more effectively than Morlet-12, which indicates a low level of stationarity and is in line with the broadness of the PSD peak. (1000-ms time window used for spectral estimation, and 100 cycle length windows for FSEM, the normalization SD was calculated from 20 to 40 Hz range in all FSEMs.)

frequencies: at low EM frequencies, there are power reductions flanking the power increase at 50 Hz, and correspondingly, at high EM frequencies, power increases can be seen on both sides of the 50-Hz power decrease. (The 100-Hz harmonic component also gives rise to a pattern similar to the 50-Hz noise, although lower in magnitude.) In the FSEM plane of the Morlet-6 (Fig. 7b), the 50-Hz component is spread wider in frequency but is of considerably lower magnitude. The band-pass of the DOG-2

wavelet is too wide for adequately describing oscillations localized in frequency, and thus the 50-Hz mains noise is poorly visible in the FSEM plane obtained with this wavelet (Fig. 7c). The evoked responses, however, are localized in time rather than in frequency and therefore are most efficiently picked up with the DOG-2. The 1200-ms constant ISI of the auditory stimulation is a specific modulation interval and represented by a curve in the FSEM plane (depicted in Fig. 7c). The evoked activity accurately follows this

curve and its harmonics. The frequency range of the evoked activity is in line with previous results (e.g., Mäkinen et al., 2004a, 2005).

Oscillatory processes were observed only in the 10- to 20-Hz range and their envelope structure differed from that of the noise specifically in the low EM frequencies. In Fig. 7d, grand-averaged FSEM planes for the three wavelets and the three window lengths are displayed. Two processes can be identified from Morlet-6 and Morlet-12 FSEMs: one coincides with the 9- to 12-Hz tau rhythm and the other occurs in the 15- to 18-Hz range. The DOG-2 wavelet does not provide sufficient frequency resolution for the separation of these processes. As indicated in Fig. 7d, the FSEMs calculated using shorter windows may be more suitable for the detection of oscillations. This follows from a higher SNR due to more segments being available for averaging with short windows. Increasing the window length, however, improves the EM frequency resolution, thus allowing a more detailed examination of the modulation structure of the signal. Both Morlet-6 and Morlet-12 FSEMs appear to yield essentially the same information on the envelope modulations with both 100 and 200 cycle windows. The envelope modulations of the 9- to 12-Hz oscillation have two maxima: one at 0.015 modulations per cycle and the other at 0.027 modulations per cycle. These correspond to respective modulation intervals of 6.8 s and at 3.7 s for 10-Hz oscillations. The 15- to 18-Hz oscillation has one maximum at 0.022 modulations per cycle, corresponding to a modulation interval of 2.8 s for 16-Hz oscillations.

In spectral estimates, six subjects displayed a peak at 9–12 Hz and one subject had a peak at 17 Hz. All seven also had prominent processes at the corresponding frequencies in the FSEM estimates (Fig. 7e). Importantly, FSEM revealed pronounced oscillatory processes (Fig. 7f), which were unobservable with spectral estimation; oscillatory processes could be reliably detected with FSEM in all 10 subjects (at least five adjacent points of probability level  $P < 0.001$ ). Three subjects displayed processes in both 9–12 and 15–18 Hz bands (at least five adjacent points of probability level  $P < 0.01$ ). Morlet-12-based FSEM, in general, provided the clearest results on the oscillations although in some cases Morlet-6 was more effective (Figs. 7e and f), which reflects the dynamics of the examined oscillations.

## Discussion

Here, we introduced new methods for detecting and analyzing oscillations buried in noise: fractally scaled envelope modulation (FSEM) estimation, which reveals even highly nonstationary neural oscillations, and partition-referenced spectral estimation (PRSE), which considerably enhances the discernibility of spectral peaks representing rhythmic activity. Envelope analysis, which is an integral part of FSEM, is commonly used in acoustics, mechanical engineering, optics, and has also been applied in some EEG and MEG studies (e.g., Clochon et al., 1996; Linkenkaer-Hansen et al., 2001, 2004). However, the current use of fractal scaling of the wavelet envelopes combined with the normalization over EM frequencies provides a novel and highly efficient method for the elemental task of detecting oscillatory processes. Moreover, FSEM yields structural information on neural activity on each frequency and facilitates compact representation of large data quantities. PRSE, then again, by removing the noise slope yields a level spectral estimate where only peaks signifying relatively stable oscillations remain. Although based on a simple technique, the

current method combined with mapping over window lengths has, to our knowledge, not been applied in brain research before: PRSE is a new technique allowing not only the observation of oscillations buried in noise but also the estimation of their duration of stationarity.

FSEM is, in several ways, superior to spectral estimation in the detection of neural oscillations: (1) Unlike spectral estimation, FSEM provides a reference level against which oscillatory processes are detected. That is, oscillatory processes are detected by virtue of the power distribution of their envelope modulations being different from the reference provided by the power distribution of noise. (2) In FSEM, each frequency is represented by a one-dimensional array (representing envelope modulation values) and the differences between noise and neural oscillation are not distributed evenly along these arrays but, rather, are likely to exhibit local maxima which facilitate the detection of oscillations. (3) FSEM is not restricted to the use of sine and cosine functions employed in spectral estimation. Rather, it is made inherently flexible by its employment of wavelets, an open-ended group of functions which may capture the examined oscillatory processes more efficiently than the Fourier basis functions. (4) FSEM does not measure the same thing as spectral estimation. A theoretical, perfectly stationary oscillation would be ideally suited for detection with spectral estimation, whereas in FSEM such an oscillation would be visible in the DC component (first bin) of the envelope frequencies (which corresponds to the power spectrum except that the Fourier basis functions are replaced by wavelets). Neural oscillations, as most natural signals, however, have continuously changing properties. In FSEM, the detection of these processes is based specifically on the changes in their properties, which again are an adverse factor for spectral estimation. However, if the signal varies over a wide range of frequencies and has irregular amplitude modulations then, correspondingly, its FSEM representations will be spread over a wide area in the frequency vs. EM frequency plane. Hence, a total lack of structure in the signal will make it unidentifiable with FSEM also.

We used FSEM and PRSE to examine MEG data from the auditory areas of the human brain. In all subjects, pronounced oscillatory processes could be detected with FSEM, while spectral estimates often provided only weak traces of this activity. At the grand-average level the spectral estimate gained without PRSE had one broad peak at 10 Hz, whereas PRSE displayed a prominent double peak (at 9.5 and 12 Hz) reflecting the distribution of single-subject spectral peaks. PRSE indicated that six out of the ten subjects displayed 9–12 Hz oscillations and one subject had an oscillation at 17 Hz. In all 10 single-subject FSEMs, oscillatory processes were observed at 9–12 or at 15–18 Hz or simultaneously in both frequency ranges. Single-subject FSEM data typically showed more pronounced oscillatory processes than the grand-averaged data. This follows from the inter-individual variability of the data, which in FSEM is spread not only along the frequency but also along the envelope-modulation-frequency axis. The current data are highly focal to auditory brain areas (via the use of planar gradiometers; Knuutila et al., 1993), but in future studies the spatial resolution may be improved by combining current methods with those developed for localizing oscillatory processes (Jensen and Vanni, 2002; Lin et al., 2004). At present, it can be noted that the 15- to 18-Hz rhythm observed here is in line with previous findings of event-related power reductions (event-related desynchronization, ERD) in auditory brain areas, which were most prominent in this frequency range (Mäkinen et al.,

2004a). Taken together, these results indicate that human auditory areas exhibit ongoing activity which varies considerably between individuals and that this activity consists of a 9- to 12-Hz tau rhythm and of a 15- to 18-Hz oscillation poorly visible in spectral estimates.

FSEM revealed that both the 9- to 12- and the 15- to 18-Hz neural oscillations exhibited maxima in their modulations at intervals of around 50 cycles (i.e., at 0.02 modulations per cycle), which explains why the modulations were visible only with the 100- and 200-cycle length windows. The locations of these modulation maxima indicate 3–7 s durations of the oscillatory states. These states span more than one epoch (but not integer multiples thereof) and are thus unlikely to be directly related to the auditory stimulation. More studies are obviously needed to clarify whether these correspond to the durations of certain perceptual states. Our results can be seen as complementing and extending previous results (Linkenkaer-Hansen et al., 2001, 2004) on envelope modulations of oscillations in sensorimotor areas. These were shown to have a  $1/f$  type of spectral distribution and to follow a power-law scaling. Our analyses performed using a high number of relatively short time windows and normalization procedures yielded a high SNR, which revealed the fine structure and local maxima in the envelope modulation spectrum.

We also observed prominent evoked responses elicited by auditory stimulation. While the frequency range where this activity occurred was clearly displayed by FSEM, it is likely that time-frequency transforms provide more informative descriptions of these processes. The current data suggested no link between evoked responses and ongoing oscillations. For example, a subject displaying exceptionally prominent auditory-evoked responses had a sole weak oscillation at around 15-Hz detectable only with FSEM (data shown Fig. 7f), whereas another subject with similarly large evoked responses displayed one of the most prominent tau rhythms (data shown in Fig. 5e). This is in line with recent findings showing that the processes generating evoked responses are distinct from those generating ongoing oscillations (Mäkinen et al., 2005; Shah et al., 2004).

The magnitude values of spectral estimates are mainly determined by the underlying noise slope, which varies according to measurement conditions and the subject. PRSE removes the noise slope and thus has the practical advantage of allowing the identification of oscillations by their peak value. This allows straightforward statistical testing and may prove useful in localizing oscillatory activity. By using simple nonlinear transforms one can use PRSE to produce ensemble or grand-averaged estimates which are not only level but where the spectral peaks are highly pronounced compared to those gained with traditional grand-averaged spectral estimates (Figs. 5d and 4, respectively). PRSE combined with mapping over window lengths may also be used for determining an effective value for the duration of the stationarity. These results, however, will be somewhat ambiguous because when the window length approaches the duration of stationarity, PRSE results can be affected by nonessential fine structure of the frequency distribution of the oscillation. Nevertheless, the method introduced here does provide a first-order estimate of the duration of the stationarity (i.e., approximately 1 s for the tau rhythm). This information can be used, for example, for selecting the optimal window length for spectral estimation.

To conclude, the methods introduced here could prove useful in a wide range of applications dealing with oscillatory processes buried in noise. In brain research, FSEM could prove beneficial not

only for the study of oscillatory brain activity per se but more generally for EEG and MEG research, for example, in the study of the processing of long-duration continuous sensory streams (Bregman, 1990). Although a stimulus stream does not have easily identifiable discrete events and does not facilitate the use of stimulus time-locked averaging, it is still likely to have a temporal structure that is represented by brain processes (Patel and Balaban, 2000, 2004). FSEM provides a high-SNR method for revealing these processes through comparing the temporal structure of the stimulus stream and the observed modulations of the neural oscillations.

## Acknowledgment

This work was supported by the Academy of Finland (project no. 173455, 1201602, 180957).

## References

- Addison, P.S., 2002. The Illustrated Wavelet Transform Handbook. IOP Press, Bristol and Philadelphia.
- Barnsley, M., 1988. Fractals Everywhere. Academic Press, Boston.
- Bastiaansen, M.C., Böcker, K.B., Brunia, C.H., de Munck, J.C., Spekreijse, H., 2001. Event-related desynchronization during anticipatory attention for an upcoming stimulus: a comparative EEG/MEG study. *Clin. Neurophysiol.* 112, 393–403.
- Bregman, A.S., 1990. Auditory Scene Analysis: The Perceptual Organization of Sound. MIT Press, Cambridge, MA.
- Clochon, P., Fontbonne, J., Lebrun, N., Etevenon, P., 1996. A new method for quantifying EEG event-related desynchronization: amplitude envelope analysis. *Electroencephalogr. Clin. Neurophysiol.* 98, 126–129.
- Cohen, L., 1995. Time-Frequency Analysis. Prentice Hall, Englewood Cliffs, NJ.
- Durka, P.J., 2003. From wavelets to adaptive approximations: time-frequency parameterization of EEG. *Biomed. Eng. Online* 2, 1.
- Freeman, W.J., 2004a. Origin, structure, and role of background EEG activity: Part 1. Analytic amplitude. *Clin. Neurophysiol.* 115, 2077–2088.
- Freeman, W.J., 2004b. Origin, structure, and role of background EEG activity: Part 2. Analytic phase. *Clin. Neurophysiol.* 115, 2089–2107.
- Hayes, M.H., 1996. Statistical Digital Signal Processing and Modeling. John Wiley & Sons, New York.
- Jensen, O., Vanni, S., 2002. A new method to identify multiple sources of oscillatory activity from magnetoencephalographic data. *NeuroImage* 15, 568–574.
- Knuutila, J.E.T., Ahonen, A.I., Hämäläinen, M.S., Kajola, M.J., Laine, P.P., Lounasmaa, O.V., Parkkonen, L.T., Simola, J.T.A., Tesche, C.A., 1993. 122-channel whole-cortex SQUID system for measuring the brain's magnetic fields. *IEEE Trans. Magn.* 29, 3315–3320.
- Krystal, A.D., Prado, R., West, M., 1999. New methods of time series analysis of non-stationary EEG data: eigenstructure decompositions of time varying autoregressions. *Clin. Neurophysiol.* 110, 2197–2206.
- Lehtelä, L., Salmelin, R., Hari, R., 1997. Evidence for reactive magnetic 10-Hz rhythm in the human auditory cortex. *Neurosci. Lett.* 222, 111–114.
- Lin, F.-H., Witzel, T., Hämäläinen, M., Dale, A., Belliveau, J., Stufflebeam, S., 2004. Spectral spatiotemporal imaging of cortical oscillations and interactions in the human brain. *NeuroImage* 23, 582–595.
- Linkenkaer-Hansen, K., Nikouline, V.V., Palva, J., Ilmoniemi, R.J., 2001. Long-range temporal correlations and scaling behavior in human brain oscillations. *J. Neurosci.* 21, 1370–1377.
- Linkenkaer-Hansen, K., Nikouline, V.V., Palva, J., Kaila, K., Ilmoniemi, R.J., 2004. Stimulus-induced change in long-range temporal correlations and scaling behaviour of sensorimotor oscillations. *Eur. J. Neurosci.* 19, 203–211.

- Mäkinen, V., May, P., Tiitinen, H., 2004a. Human auditory event-related processes in the time-frequency plane. *NeuroReport* 15, 1767–1771.
- Mäkinen, V., May, P., Tiitinen, H., 2004b. Spectral characterization of ongoing and auditory event-related brain processes. In: Halgren, E., Ahlfors, S., Hämäläinen, M., Cohen, D. (Eds.), *Proceedings of the 14th International Conference on Biomagnetism*, Boston, pp. 521–522.
- Mäkinen, V., Tiitinen, H., May, P., 2005. Auditory event-related responses are generated independently of ongoing brain activity. *NeuroImage* 24, 961–968.
- Mallat, S.A., 1998. *Wavelet Tour of Signal Processing*. Academic Press, San Diego.
- Mandelbrot, B.B., 1999. *Multifractals and  $1/f$  Noise*. Springer-Verlag, New York.
- Pardey, J., Roberts, S., Tarassenko, L., 1996. A review of parametric modelling techniques for EEG analysis. *Med. Eng. Phys.* 18, 2–11.
- Patel, A.D., Balaban, E., 2000. Temporal patterns of human cortical activity reflect tone sequence structure. *Nature* 404, 80–84.
- Patel, A.D., Balaban, E., 2004. Human auditory cortical dynamics during perception of long acoustic sequences: phase tracking of carrier frequency by the auditory steady-state response. *Cereb. Cortex* 14, 35–46.
- Pfurtscheller, G., Lopes da Silva, F.H. (Eds.), *Event-Related Desynchronization*. Handbook of Electroencephalography and Clinical Neurophysiology. Elsevier, Amsterdam.
- Shah, A.S., Bressler, S.L., Knuth, K.H., Ding, M., Mehta, A.D., Ulbert, I., Schroeder, C.E., 2004. Neural dynamics and the fundamental mechanisms of event-related brain potentials. *Cereb. Cortex* 14, 476–483.
- Torrence, C., Compo, G.P., 1998. A practical guide to wavelet analysis. *Bull. Am. Meteorol. Soc.* 79, 61–78.
- Varela, F.J., Lachaux, J.P., Rodriguez, E., Martinerie, J., 2001. The brainweb: phase synchronization and large-scale integration. *Nat. Rev., Neurosci.* 2, 229–239.
- Yeung, N., Bogacz, R., Holroyd, C.B., Cohen, J.D., 2004. Detection of synchronized oscillations in the electroencephalogram: an evaluation of methods. *Psychophysiology* 41, 822–832.